CO$_2$ Separation by Imide/Imine Organic Cages

Sonia La Cognata+,[a] Riccardo Mobili+,[a] Chiara Milanese,[a] Massimo Boiocchi,[b] Mattia Gaboardi,[c] Donatella Armentano,[d] Johannes C. Jansen,*[e] Marcello Monteleone,[e] Ariana R. Antonangelo,[f] Mariolino Carta,*[f] and Valeria Amendola*[a]

Abstract: Two novel imide/imine-based organic cages have been prepared and studied as materials for the selective separation of CO$_2$ from N$_2$ and CH$_4$ under vacuum swing adsorption conditions. Gas adsorption on the new compounds showed selectivity for CO$_2$ over N$_2$ and CH$_4$. The cages were also tested as fillers in mixed-matrix membranes for gas separation. Dense and robust membranes were obtained by loading the cages in either Matrimid® or PEEK-WC polymers. Improved gas-transport properties and selectivity for CO$_2$ were achieved compared to the neat polymer membranes.

Introduction

The growing concern about global warming is stirring worldwide interest in materials and technologies for pre- and post-combustion CO$_2$ capture and for clean energy production.[1,2] Among the technologies currently applied, membrane-based separation is more cost-effective and energy-efficient, but suffers from a well-known trade-off between permeability and selectivity.[3,4] This point has recently been addressed by incorporating intrinsically porous materials (IPMs), selective for gases of interest, into polymeric membranes. The resulting

[a] Dr. S. La Cognata,+ Dr. R. Mobili,+ Prof. C. Milanese, Prof. V. Amendola
Department of Chemistry, University of Pavia
Viale Tarquato Taramelli 12, Pavia, 27100 (Italy)
E-mail: valeria.amendola@unipv.it

[b] Dr. M. Boiocchi
Centro Grandi Strumenti, University of Pavia
Via Bassi 21, Pavia, 27100 (Italy)

[c] Dr. M. Gaboardi
Elettra sincrotrone Trieste S.C.p.a.
Area science park, Basovizza (TS), 34149 (Italy)

[d] Prof. D. Armentano
Department of Chemistry & Chemical Technologies
University of Calabria
Via P. Bucci, 13/C, 87036 Rende (CS) (Italy)

[e] Dr. J. C. Jansen, Dr. M. Monteleone
Institute on Membrane Technology
National Research Council of Italy (CNR-ITM)
Via P. Bucci 17/C, Rende (CS), 87036 (Italy)
E-mail: johannescarolus.jansen@cnr.it

[f] Dr. A. R. Antonangelo, Dr. M. Carta
Department of Chemistry
College of Science, Swansea University
Singleton Park, Swansea, Wales, SA2 8PP (UK)
E-mail: mariolino.carta@swansea.ac.uk

[+] These authors contributed equally to this manuscript.

mixed-matrix membranes (MMMs) can boost the performance of neat membranes by combining the scalability and processability of polymers with the selectivity of fillers.[5] Among the investigated IPMs, molecular materials[6] – such as organic cages[7,8] and macrocyclic compounds[9] – have the advantage of being more soluble in organic solvents (compared to, e.g., metal-organic and covalent organic frameworks)[10–12] and therefore more easily processable in the preparation of MMMs.[13] One of the first successful attempts to obtain MMMs, using porous organic cages (POCs)[7] as fillers, was achieved by crystallizing the cage molecules within the polymer membrane.[14] The resulting MMMs showed enhanced permeability and resistance to physical aging. Significant enhancements of both permeability and selectivity were achieved by embedding a mixture of amorphous POCs into a composite membrane.[15] In this case, a fourfold improvement in permeability was reached for CO$_2$, N$_2$, and CH$_4$.

Over the last decades, organic cages such as azacryptands have been extensively studied in molecular recognition as selective hosts for, for example, pollutants and drugs in aqueous solution and complex matrices.[16–18] Following the seminal work by Cooper et al. in 2009, cages have also gained interest as porous materials for gas capture and separation. In fact, beside their intrinsic cavity, POCs can display extrinsic and interconnected pores deriving from their packing in the solid state. For gas uptake and separation applications,[19–23] POCs have been studied as either crystalline or amorphous/glassy solids,[7,24,25] and more recently in the liquid state.[26] Over the last few years, POCs with different geometries (e.g., cubic,[27] prismatic,[28] tetrahedral[29,30]) have been developed; in most cases, the dynamic covalent chemistry approach (e.g., imine condensation, alkyne metathesis, boronate ester formation, etc.)[31] was applied for their syntheses.

The most common POCs are probably the systems obtained by imine condensation between suitably designed polyaldehydes and polyamines.[9,32,33] The [4 + 6] imine cages reported by Mastalerz et al.,[8] for instance, display porosity features that are comparable to those achieved with some covalent organic frameworks. The selectivity for CO$_2$ vs. N$_2$ (or CH$_4$) can be

Chemistry–A European Journal

Research Article
doi.org/10.1002/chem.202201631

Chemistry Europe
European Chemical
Societies Publishing

efficiently enhanced in macrocyclic hosts and cages by decorating their cavity with heteroatoms (e.g., O, N), polar groups (e.g., phenol, pyrrole, carbonyl)[34–36] or π-acceptor moieties,[37] that can establish hydrogen bonding or dipole-quadrupole interactions with CO_2. A high affinity for CO_2 was obtained, for example, by means of urea-based cucurbituril macrocycles.[6,38] X-ray diffraction studies on the hydrogen-bonded framework generated by curcubit[6]uril molecules (CB[6]), revealed that the adsorbed CO_2 molecules interact with the carbonyls of the CB[6] units, and establish H-bonds with the C−H groups of CB[6] walls, exhibiting a CO_2 heat of adsorption of 33 kJ mol^{-1}.

Among porous cages, imide-based systems recently showed interesting gas adsorption features. In particular, the soft porous crystals of the polymorphic cage obtained by condensation of a flexible polyamine with a rigid dianhydride showed a peculiar CO_2-induced breathing behavior.[39] The interaction of CO_2 with the cage cavity promoted the reversible switching of the cage material from a "closed" nonporous phase to a gate-open structure. On the other hand, the imide/imine cages reported by Coskun et al.[40] showed shape-persistence in the solid state and a high affinity for CO_2. The cage containing pyromellitic diimide units, in particular, featured a good selectivity for CO_2 versus N_2 (i.e., 45.5 at 273 K), as demonstrated by applying the ideal adsorbed solution theory (IAST)[41] to gas-adsorption studies results.

In this work, we report two novel imide/imine organic cages (see **C1** and **C2** in Scheme 1), prepared by [2+3] imine condensation of two different polyamines with a novel dialdehyde compound, containing the rigid bicyclo[2.2.2]oct-7-ene-2,3,5,6-tetracarboxydiimide core. We chose to investigate this type of cages because the large number of heteroatoms and polar groups on their framework could increase the selectivity for CO_2 with respect to N_2 and CH_4. We employed the bicyclic bridge-based dialdehyde for the synthesis because its bent structure could have a positive effect on the formation of a cage, disfavoring the possible formation of oligomers/polymers (this was confirmed by our results). Gas-adsorption studies on the cage materials showed a good selectivity for CO_2

over N_2 (for carbon capture and storage) and CH_4 (for biogas upgrading) at 1–5 bar, which are the typical pressures employed during vacuum swing adsorption (VSA). The cages were also tested as fillers in MMMs, using either Matrimid® or PEEK-WC as the polymer matrix. Preliminary studies with CO_2, N_2, and CH_4 pointed out an improvement of the gas-transport properties of the MMMs compared to the neat polymer membranes.

Results and Discussion

Synthesis and characterization

C1 and **C2** were synthesized by imine condensation of either N,N-bis(2-aminoethyl)ethylenediamine (tren) or the 1,3,5-tris(aminomethyl)-2,4,6-triethylbenzene (for **C1** and **C2**, respectively) with a bis(dicarboximide)-based dialdehyde (see details in the Supporting Information). Both cages precipitated as pure solids from the reaction mixture in acetonitrile (MeCN) as a solvent, and the structures were confirmed by ^{1}H and ^{13}C NMR spectroscopies (see Figures S28-S38). Elemental analysis allowed us to determine the formula of the two compounds: $C_{90}H_{78}N_{14}O_{12} \cdot 4H_2O$ for **C1**; $C_{108}H_{96}N_{12}O_{12} \cdot 2H_2O$ for **C2**.

Scanning electron microscopy (SEM) images suggest that the **C1** cage precipitated as a mixture of an amorphous material in nanometric form and larger prismatic crystals (Figure S1, while **C2** showed a crystalline prismatic well-defined morphology (Figure S5). Higher crystallinity of **C2** compared to **C1** was confirmed by powder X-ray diffraction (PXRD) analysis (Figures S2 and S6).

The Fourier transform infrared spectroscopy-attenuated total reflectance (FTIR-ATR) spectra of the two compounds show the typical C═N stretching features at 1644 and 1636 cm^{-1} respectively for **C1** and **C2** (Figures S3 and S7). Peaks assigned to the diimide groups (i.e., symmetric and asymmetric stretching of C═O) appear at 1704 and 1774 cm^{-1} for **C1**, 1709 and 1779 cm^{-1} for **C2**.
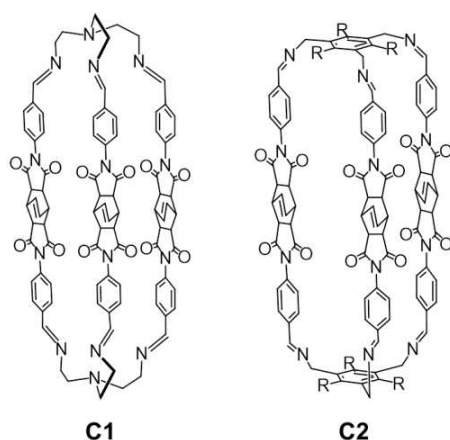
The thermal stability of **C1** and **C2** was assessed through thermogravimetric analysis (TGA). Apart from a small weight loss for the **C1** sample, very likely from humidity, **C1** and **C2** showed decomposition only starting from around 220 and 330 °C, respectively (Figures S4 and S8).

Single-crystal X-ray diffraction (SCXRD) studies

Single crystals suitable for XRD study were obtained for both **C1** and **C2**.

Crystals of the compound of formula $C_{90}H_{78}N_{14}O_{12} \cdot 2MeCN \cdot H_2O$ crystallize in the monoclinic system (**C1**-α, $P2_1$; $a = 19.1383(13)$ Å, $b = 11.6804(8)$ Å, $c = 19.3415(14)$ Å, $\beta = 92.2030(10)°$, $V = 4320.5(5)$ Å^3) and were formed by slow evaporation of a solution of **C1** in MeCN.

As revealed by the SCXRD analysis of this crystalline **C1**-α phase (see the Supporting Information for details), each molecular cage assumes an elongated conformation with

Scheme 1. Sketches of **C1** and **C2** (R = ethyl).

Chemistry–A European Journal

Research Article
doi.org/10.1002/chem.202201631

Chemistry Europe
European Chemical
Societies Publishing

collapsed cavity (Figure 1). The distance between the apical tertiary amines measures approximately 22 Å, and the bicyclo[2.2.2]oct-7-ene containing groups are oriented so as to point their HC=CH towards the cavity centre. The average shortest intramolecular separation between the HC=CH hydrogens of the three cage-arms is about 3.0 Å. This closed conformation is stabilized by intramolecular H-bonding interactions between carbonyl oxygens and hydrogen atoms (aryl-H; Figure S9) of different cage arms. The asymmetric unit contains three crystallization solvent molecules (two acetonitrile and one water), as shown by the formula, that occupy extrinsic pores.

The cages are tightly packed, generating a thick network of intermolecular H-bonds (Figure 2). These involve the carbonyl oxygens as H-acceptors, and the C_{aryl}-H and C_{sp^3}–H bonds of
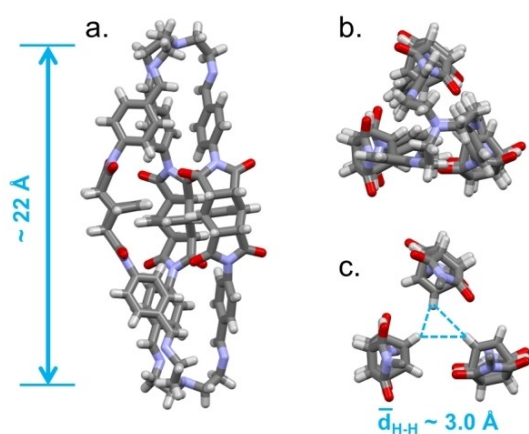
bicyclo[2.2.2]oct-7-ene-based spacers as H donors. Geometrical features of these weak C–H···O interaction are reported in Table S2. Considering the crystal structure without guest molecules, the calculated voids accessible to a molecular probe of 1.72 Å radius (generally used for CO_2)[42] only correspond to 0.1% of unit cell volume (Figure 2, see the Supporting Information for details).[43] The calculated PXRD pattern of **C1**-α was compared to the experimental one acquired on the microcrystalline powder of formula $C_{90}H_{78}N_{14}O_{12} \cdot 4 H_2O$, precipitated from the reaction mixture, and used in the studies with gases (Figure S2). Although the calculated diffraction peaks of **C1**-α can be recognized in the experimental pattern, this is dominated by the "halo" of an amorphous component. Undoubtedly, the effect of the lattice solvent plays a crucial role in supporting the ordered crystal packing, anyway we can speculate that the phase of the bulk solid corresponds to the structure reported in Figures 1 and 2.

In the case of **C2**, by slow cooling of a saturated solution of the cage in dimethyl sulfoxide (DMSO), we obtained crystals corresponding to the formula $C_{108}H_{96}N_{12}O_{12} \cdot 11 DMSO \cdot 5 H_2O$ which crystallized in the monoclinic system (**C2**-β, P2₁/n; $a = 24.354(3)$ Å, $b = 20.120(2)$ Å, $c = 31.705(3)$ Å, $\beta = 109.434(5)$, $V = 14650(3)$ Å³; Figure 3. As the crystals proved very fragile and unstable outside of their mother liquor, especially at room temperature, SCXRD data were collected at 190 K. Any attempt to measure them at lower temperatures (in the range 90–170 K) failed due to the collapse of the crystalline lattice. The crystal structure (see below) finally unveiled that the very large amount of lattice DMSO molecules was most likely at the origin of the intrinsic fragility. A thermal shock originates the collapse of the crystalline phase in consequence to the failure of the required fast ordered rearrangement in the supramolecular motifs involving DMSO. Analysis of the data showed that, compared to the empty and collapsed **C1** cage, the cavity of **C2** is open, large, and filled with crystallization molecules. The cage has an elongated prolate spheroid shape with a separation between the triethylaryl platforms of about 20 Å (calculated by the

Figure 1. a) Front and b) top views of the crystal structure of **C1** in **C1**-α crystals; MeCN and water molecules are omitted for clarity. c) Focus on the central portion of the cage cavity (top view), dashed cyan lines show minimum distances between HC=CH hydrogens.
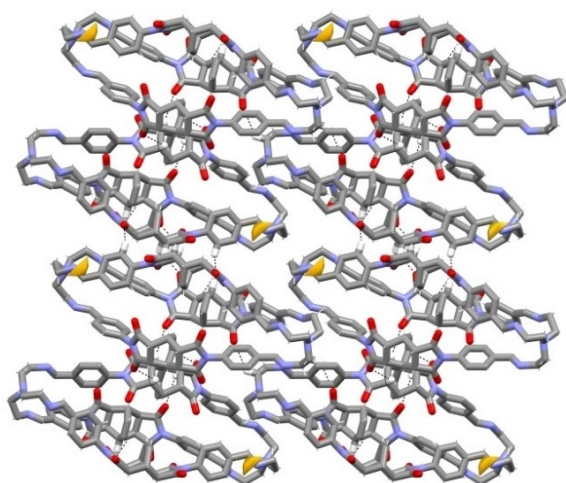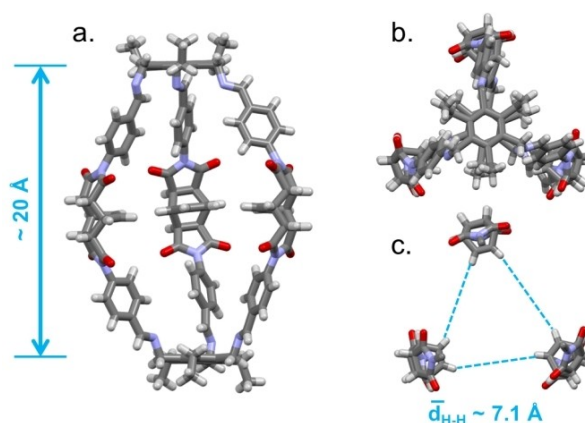

Figure 2. A view of the packing along the b crystallographic axis, for the **C1**-α phase (MeCN and crystallization water molecules have been omitted for clarity). The free volume, as determined by the solvent-accessible surface for a molecular probe of 1.72 Å radius, is reported in yellow.[43] H-bonding interactions are highlighted as dashed lines. H atoms are drawn as small sticks, except for the ones involved in C–H···O hydrogen bonds.

Figure 3. a) Front and b) top views of the crystal structure of **C2** in **C2**-β; DMSO and water molecules are omitted for clarity; c) Focus on the central portion of the cage cavity (top view), dashed cyan lines show minimum distances between HC=CH hydrogens.

Chemistry–A European Journal

Research Article
doi.org/10.1002/chem.202201631

Chemistry Europe
European Chemical
Societies Publishing

centroid-centroid distance). The HC≡CH bonds of the bicyclo[2.2.2]oct-7-ene containing spacers point towards the cage cavity, and the average separation between the HC≡CH hydrogens measures 7.1 Å. In the **C2**-β phase, adjacent cages are involved in weak C−H···O interactions having the carbonyl oxygens as H-acceptors, and C_{aryl}−H, C_{sp^2}−H, and C_{sp^3}−H as H-donors; their geometrical features are reported in Table S2. However, the cage packing is less dense compared to **C1**-α and, as previously mentioned, many additional guest solvent molecules co-crystallized within the pores. In fact, the unit cell totally contains 16 crystallization solvent molecules (11 DMSO, 5 H_2O), which is significant compared to the three found in the unit cell of **C1**-α (2 MeCN, 1 H_2O).

For the crystal structure without guest molecules, the calculated voids correspond to 9.8% of unit cell volume (Figures 4 and S10).[43] It is worthwhile mentioning that, as expected, the calculated PXRD pattern for the **C2**-β phase is clearly different from the experimental one (Figure S6), recorded on the microcrystalline phase of formula $C_{108}H_{96}N_{12}O_{12}\cdot2\,H_2O$ (from now on called **C2**-γ).

New crystals, suitable for SCXRD, were also obtained from a saturated solution of **C2** in MeCN. Single-crystal data were collected at 300 K on the XRD2 beamline[44] at the Elettra synchrotron light-source (Trieste, Italy) at a wavelength of 0.6199 Å. In this solvent, **C2** crystallizes forming a triclinic phase (hereafter **C2**-δ) containing two molecules as asymmetric unit ($Z=6$; s.g. $P\bar{1}$; $a=14.423(3)$ Å, $b=25.413(5)$ Å, $c=32.957(7)$ Å, $\alpha=85.77(3)°$, $\beta=78.52(3)°$, $\gamma=78.30(3)°$; $V=11585(4)$ Å^3). At 300 K, the solvent trapped in the **C2**-δ cavities is in a disordered form. A solvent mask was calculated, and 768 electrons were found in a volume of 3648 Å^3 in two voids per unit cell. This is consistent with the presence of about 5.8 MeCN molecules per asymmetric unit, which account for 770 electrons per unit cell, or $C_{108}H_{96}N_{12}O_{12}\cdot3\,MeCN$. The average separation between the
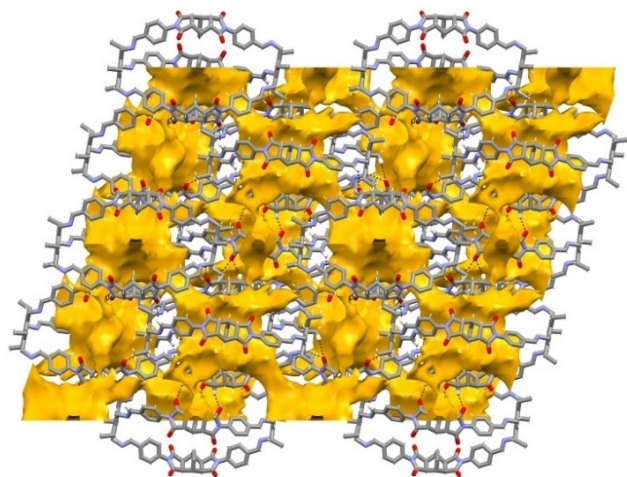

Figure 4. A view of the packing along the *b*-axis for the **C2**-β phase, obtained by omitting DMSO and water crystallization molecules. The free volume is reported in yellow, as calculated by the solvent-accessible surface for a molecular probe of 1.72 Å radius; H-bonding interactions are highlighted by dashed lines. H-atoms are drawn as small sticks, except for the ones involved in C−H···O hydrogen bonds.

HC≡CH hydrogens is calculated to be 6.1 Å for the single molecule, with a standard deviation of 1.66 Å. However, **C2** molecules in phase **C2**-δ form partly entangled dimers (the single cages are highlighted in blue and yellow, in Figure 5) and the effective inner radius will be smaller than that expected for a single molecule. Comparing **C2**-β and **C2**-δ crystal structures, it is worth noting that the latter crystallizes with a cage molecule (yellow in Figure 5) exhibiting one of the external CH_3 groups oriented facing toward the inner void, while the structure of the second molecule (blue in Figure 5) is like that of **C2**-β. In addition, the cage molecules are more densely packed in **C2**-δ than in the **C2**-β phase, and the calculated voids potentially accessible to CO_2 are reduced to 1.9% of unit cell volume (Figure S11). As found for **C2**-β, the calculated PXRD pattern is different from the experimental one recorded on **C2**-γ (Figure S6).

Gas-adsorption studies on C1 and C2

Gas-adsorption studies were performed on **C1** and **C2** using CO_2, N_2, and CH_4 as probe gases. As already anticipated, the **C1** solid, as precipitated from the reaction mixture, was principally amorphous. On the other hand, **C2** was collected as a microcrystalline powder, **C2**-γ.

Before performing gas sorption studies, **C1** and **C2** samples were homogenized in a ball-mill, and then activated by heating overnight at 350 K under vacuum to remove traces of humidity.

Brunauer-Emmett-Teller surface areas (SA_{BET}) were initially determined using N_2 as the probe gas. The isotherm curves showed little N_2 adsorption at 77 K (Figures S17 and S18). The BET surface areas were calculated at a relative pressure $p/p_0 < 0.1$ showing i) an apparent surface area of ∼44 m^{2}g^{-1} and a pore volume of 3.4×10^{-2} cm^{3}g^{-1} for **C1**; ii) an apparent surface area of ∼35 m^{2}g^{-1} and a pore volume of 8.2×10^{-2} cm^{3}g^{-1} for **C2**. The interpretation of the isotherms and the data suggest that both materials are either nonporous or that the pores are buried and not readily accessible, especially at 77 K, where the adsorption kinetic is very slow. The pronounced hysteresis may support the second option (Figures S12 and S13).[45,46] The N_2 adsorption was also measured at room temperature (298 K).
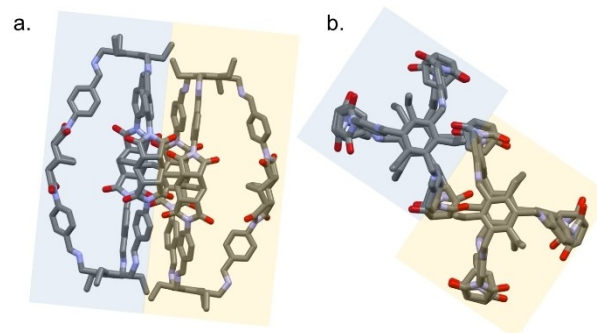

Figure 5. a) Front and b) top views of the two cage molecules per asymmetric unit (highlighted in blue and yellow) of the **C2**-δ phase. Hydrogens and solvent molecules are omitted for clarity.

Chemistry–A European Journal

Research Article
doi.org/10.1002/chem.202201631

**Chemistry
Europe**
European Chemical
Societies Publishing

This is important when used to calculate the selectivity over CO_2, to simulate post-combustion conditions that are normally reported at room temperature. As expected, the adsorption at this temperature is much lower than that at 77 K, with relatively low or almost no adsorption up to 1 bar (Figure S14).

To assess the affinity for CO_2 and the separation selectivity over N_2 and CH_4, the CO_2 uptake was measured at both 273 and 298 K. The lower temperature is also crucial to assess the pore size distribution (PSD)[46,47] by both nonlocal density functional theory (NLDFT) and Horvath-Kawazoe (H–K) methods. NLDFT is considered one of the most reliable methods to evaluate PSD, and certainly the one that gives more information about the contribute of each different pore size. PSD is preferably assessed by CO_2 adsorption at 273 K over N_2 at 77 K, as the latter cannot penetrate pores smaller than 5 Å whereas CO_2 allows the evaluation of pores ~3.5 Å, which is considered as the ultra-microporous region.[46,48,49]

At 273 K, **C1** and **C2** samples exhibited a CO_2 uptake of ~17.9 $cm^3 g^{-1}$ (0.799 $mmol g^{-1}$) and ~26 $cm^3 g^{-1}$ (1.161 $mmol g^{-1}$), respectively. Despite these values not being very high, the uptake is much larger than what we expected from the low N_2 adsorption. The CO_2 isotherms (Figures S15 and S16) show a less pronounced hysteresis than the N_2 curves. This suggests that the materials are somewhat porous after all, but it also confirms that the pores may be poorly accessible to be measured with N_2. It is also possible that the higher temperature (273 K for CO_2 vs. 77 K for N_2) produced some swelling of the flexible parts of the cages, which permits a higher and a faster kinetic adsorption of CO_2 compared to N_2.[50,51] The potential deformation of the cages may also account for the relatively good CO_2 adsorption for **C1**, which seemed unlikely by simply looking at the volume calculated by crystal structure analysis.

The calculation of the BET surface area from the CO_2 curve is more unusual than from N_2, but feasible and reliable.[50] It showed SA_{BET} of 224 $m^2 g^{-1}$ for **C1** and 325 $m^2 g^{-1}$ for **C2** (at 273 K). These results are in line with those obtained in similar conditions by Sessler et al. for cryptand-like cages, containing multi-pyrrolic units as structural components (Table S3).[34]

The measurements of CO_2 at 298 K showed the expected reduction in the uptake (~13.6 $cm^3 g^{-1}$, 0.607 $mmol g^{-1}$ for **C1**; ~15.5 $cm^3 g^{-1}$, 0.692 $mmol g^{-1}$ for **C2**) but the decrease is not as steep as we expected, which may suggest some contribution from chemisorption. This could be easily due to the presence of heteroatoms, polar and H-bonding groups in the structures, which are known to enhance the affinity for CO_2.[39]

Heats of adsorption (Q_{st}) were calculated from the CO_2 isotherms measured at 273 and 298 K. The curves were fitted with the Langmuir-Freundlich equation and the Q_{st} calculated using the Clausius-Clapeyron equation[52] at zero coverage. The data showed approximate values of 35 KJ mol^{-1} for **C1** and 39 KJ mol^{-1} for **C2**, which suggests that the main adsorption mechanism is driven by physisorption, although we cannot exclude a little contribution from chemisorption (which is considered for values >30 KJ mol^{-1}). Notably, these Q_{st} values are comparable to those obtained with cucurbituril

macrocycles,[6] and are indicative of the high affinity of the investigated materials for CO_2.

The calculation of the pore size distribution by NLDFT from CO_2 at 273 K, reveals that both materials show a series of pores centered at 3.5, 5.0 and 8.2 Å (see the Supporting Information for details). In the case of **C1**, the very small peak at ~3.5 Å suggests little ultra-microporosity. The low overall pore volume centered at that height (<0.1 $cm^3 nm^{-1} g^{-1}$) confirms the relatively low surface area. For **C2**, the peak at ~3.5 Å is more pronounced, sign of a slightly higher ultra-microporosity contribution. Despite the pore size distribution is considered as merely qualitative, the scattered distribution of peaks and the low amount of ultra-micropores confirm that both materials are not very porous and that the accessibility for the gases may be hindered. The H–K model showed only the main peak centered at ~6 Å. The peak is cut after that range, which is typical of the H–K measurements with CO_2 at 1 bar of maximum pressure and exposes the limitations and the lack of information of this calculation over the more reliable NLDFT.

Comparison of the curves derived from the isothermal gas adsorption measurements at 298 K for CO_2, N_2 and CH_4, provides interesting insight into the potential use of these materials for post-combustion separation (Figure 6).[53] The amount of CO_2 adsorbed largely exceeds the amount of N_2. Even just visually, we can expect **C2** having a better selectivity than **C1**, but the calculation for a possible post-combustion separation cannot be done simply looking at the final uptake of the two gases at 1 bar. The first step of the calculation of the selectivity of a hypothetical CO_2/N_2 mixture is done by fitting the curves with the IAST method.[41] In our case they were fitted from a dual-site Langmuir-Freundlich equation using the IAST++ software.[54]

The second step consists of the calculation of the ideal selectivity, assuming a 15% CO_2 and 85% N_2 gas mixture, which simulates the typical flue gas composition that is used to separate CO_2 and N_2 during post-combustion carbon capture using VSA.[55] The final selectivity is taken from the curve
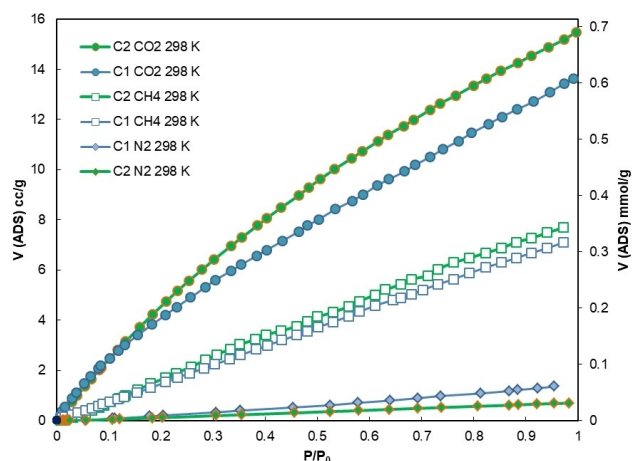

Figure 6. Overlay of CO_2, CH_4, and N_2 adsorption isotherms, measured at 298 K. **C1** (blue) and **C2** (green). $p_0 = 1$ bar, which is the maximum pressure reached by the instrument.

Chemistry–A European Journal

Research Article
doi.org/10.1002/chem.202201631

Chemistry
Europe
European Chemical
Societies Publishing

approaching 1 bar, as this is the typical pressure for post-combustion by VSA and the maximum that our instrument can reach (Figures S23 and S24).

The selectivity of **C1** and **C2** for this separation demonstrated competitive compared to similar reported cages (Table S3) and other porous materials.[6,56] Analysing the data, we observed that the **C1** material is slightly more selective than **C2** (41 vs. 32, Table 1). This is most likely due to its smaller pores and lower BET surface that leads to an improved molecular sieving effect. The two solids were also tested for the potential separation of CO_2 from CH_4, simulating biogas upgrading (i.e., the removal of CO_2 from a mixture to improve the efficiency of CH_4 as a fuel), which can be also performed by VSA[57] at 1 bar. According to the operating conditions typically reported for this separation, the CO_2/CH_4 selectivity was simulated assuming a 50/50%$_v$ composition. Usually, the selectivity for this gas pair is lower than the correspondent CO_2/N_2 for the same materials.[58] This trend is confirmed by the results herein obtained, as **C1** proved again more selective than **C2** but with much lower values compared CO_2/N_2 (5.3 for **C1** vs. 3.0 for **C2**).

C1 and C2 as fillers in MMMs

The selectivity results achieved with the IAST simulation encouraged us to verify the possibility of employing our cages as fillers for MMMs for gas separation. With this is in mind, we tested our novel materials with two different polymer matrices, the commercial polyimide Matrimid® 9725 and poly(ether-ether ketone) with cardo group, PEEK-WC, that are both commonly used polymers for gas separation membranes (Scheme 2).[59,60]

For the preparation of MMMs, we followed the experimental procedure recently employed by our group in the development of MMMs containing azacryptands as fillers.[61] In particular, the cages were firstly homogeneously dispersed in chloroform, then the required amount of polymeric solution (2 wt.% Matrimid® 9725 or 3 wt.% PEEK-WC in chloroform) was added. **C1** and **C2**, were loaded in the polymer matrix at 20 wt. % based on the total mass of the membranes.

The resulting mixture was sonicated, and then poured into a Teflon petri dish. Dense membranes were obtained by slow evaporation of the solvent at 25 °C for 24 h. The resulting MMMs were removed from the Petri dish and their top surface was coated with PDMS Elastosil M 4601 (prepolymer + cross-linker) to cover possible pinhole defects. Further details on MMMs preparation are reported in the Supporting Information,
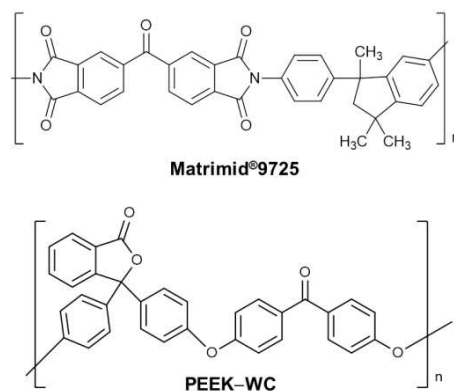
Scheme 2. Chemical structures of Matrimid®9725 and PEEK-WC.

while details of the coating procedure were reported elsewhere.[61]

Pure gas permeation tests were performed at 298 K, and at a feed pressure of 1 bar in a fixed volume/pressure increase setup using the time-lag method for the determination of the permeability (P), diffusion (D), and solubility coefficients (S). Details of the instrument and the measurement procedure were reported elsewhere.[62]

The Robeson plots (Figure 7) show the permeability and selectivity data for the two most interesting gas pairs, CO_2/CH_4 and CO_2/N_2. These plots, in which, for example, the selectivity for CO_2 versus N_2 is plotted against the CO_2 permeability (Figure 7a), are generally used to compare the performance of different materials with respect to the state of the art.[63,64] In particular, the Robeson plots in Figure 7 compare the performance of our MMMs (i.e., green diamond, Matrimid® 9725/**C1**; green square, Matrimid® 9725/**C2**; red diamond, PEEK-WC/**C1**; red square, PEEK-WC/**C2**) and of the neat polymers (green and red circles for Matrimid® 9725 and PEEK-WC, respectively) with the best performance achieved for a given separation, as defined by the upper bounds (see the diagonal lines in Figure 7).

Notably, **C1** and **C2** have opposite effects on the CO_2 permeability (Table 2). In particular, the addition of **C1** as filler results in a marginal decrease of the CO_2 permeability in Matrimid (green diamond vs. green circle in Figure 7), and an approximately $1/3$ decrease in PEEK-WC (red diamond vs. red circle). On the other hand, **C2** increases the CO_2 permeability by few percent in PEEK-WC (Table 2; red square vs. red circle in Figure 7) and about 50% in Matrimid® 9725 (green square vs.

Table 1. CO_2 adsorption studies on **C1** and **C2**.					
Cage	SA_{BET, CO_2}[a] [m^2 g^{-1}]	V_{ADS,CO_2}[b] [cm^3 g^{-1}]	V_{ADS,CO_2}[c] [cm^3 g^{-1}]	Q_{ST} [kJ mol^{-1}]	CO_2/N_2[d] (IAST)
C1	224	17.9	13.6	35	41
C2	325	26.0	15.5	39	32
[a] BET surface areas (SA_{BET}) calculated for CO_2 at 273 K over the p/p_0 range 0.01–0.1; [b] and [c] CO_2 uptake at 273 and 298 K, respectively (1 bar). [d] selectivity of CO_2 over N_2 adsorption (IAST, 298 K for a CO_2/N_2 15:85 composition).					

Chemistry–A European Journal

Research Article
doi.org/10.1002/chem.202201631

Chemistry Europe
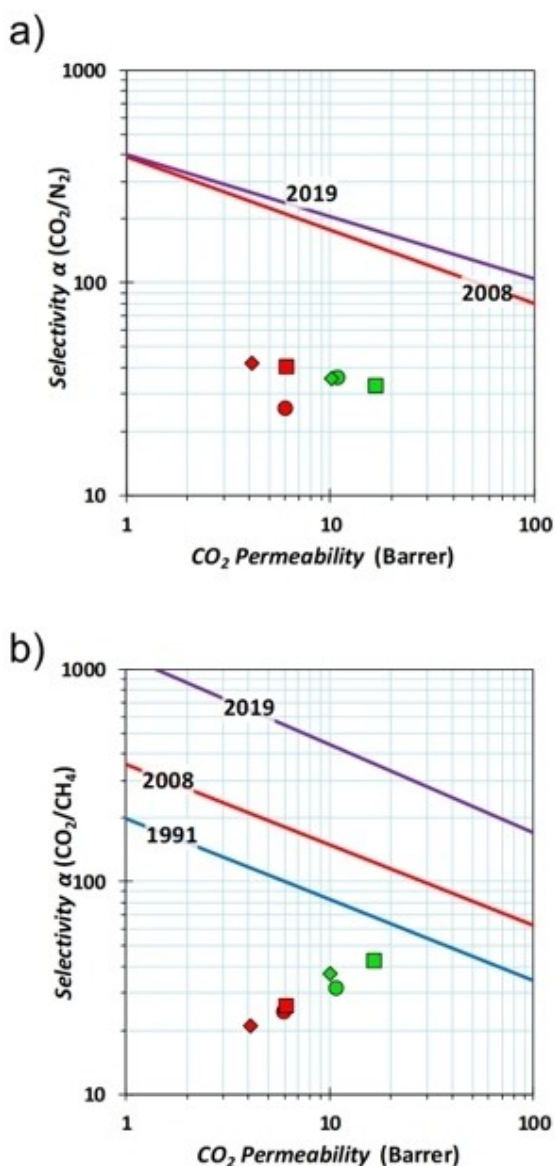European Chemical
Societies Publishing

Figure 7. Robeson plots for the a) CO_2/N_2, b) CO_2/CH_4, gas pairs. Blue and red lines correspond to 1991 and 2008 upper bounds, respectively.[63,64] The purple line corresponds to the 2019 upper bound.[66] The data are reported as: ●: Matrimid® 9725, ■: Matrimid® 9725/**C2**, ◆: Matrimid® 9725/**C1**, ●: PEEK-WC, ■: PEEK-WC/**C2**, and ◆: PEEK-WC/**C1**.

ity for **C1** and the increase for **C2** suggest that the fillers have a lower and higher permeability than the polymers, respectively.[61] This is also in line with the lower porosity of **C1** compared to **C2**, resulting from the gas-adsorption studies on the two materials (see, e.g., SA_{BET, CO_2} values at 298 K in Table 1).

As for selectivity, both **C1** and **C2** significantly increase the CO_2/N_2 selectivity in PEEK-WC (Table 2 and Figure 7a). Improved CO_2/CH_4 selectivity is also found for the PEEK-WC/**C2** membrane (Figure 7b). Noticeably, both cages increase the CO_2/CH_4 selectivity in Matrimid® 9725 but did not affect the CO_2/N_2 selectivity (**C1**) or slightly decrease it (**C2**).

These changes are associated with a general increase of the effective diffusion coefficient by **C2** in both polymers (Table 3), especially for the gas with small molecular diameter. Instead, **C1** increases the diffusion coefficient in PEEK-WC, but reduces it in Matrimid® 9725.

In PEEK-WC, these changes are also accompanied by an increase in size-selectivity, as the slope of the correlation of $\log(D)$ versus the squared gas diameter (d^2_{eff}) increases with both cages (see the red lines in Figure 8a). On the other hand, the cages have negligible effect on the size-selectivity in Matrimid® 9725 (Figure 8b). The differences between the two cages can be ascribed to the higher porosity of **C2**.

Conclusion

Two novel imide/imine-based organic cages are reported in this work. The systems were investigated as materials for gas-separation processes both as pure solids and loaded in polymeric membranes.

SCXRD analyses showed that both cages crystallize to form a thick network of intermolecular H-bonds, which principally involve the bicyclo[2.2.2]oct-7-ene-based spacers (the carbonyl oxygens and the C_{aryl}—H/C_{sp^3}—H bonds, in particular) of different cage molecules. The thick packing significantly reduces the free volume potentially accessible to gases in the crystal. In fact, when a molecular probe of 1.72 Å radius was considered, the calculated voids represented only 0.1 and 9.8% of unit cell volume for **C1** and **C2**, in **C1**-α and **C2**-β phases, respectively.

The crystalline materials could not be produced in a large enough quantity to allow us to perform studies with gases. These investigations were therefore conducted on the solids precipitated from the reaction mixtures, and then ball-milled to achieve materials that could be homogenously dispersed into polymer matrices for the preparation of MMMs. PXRD analyses

green circle). On the basis of the Maxwell equation (see the Supporting Information for details), the decrease in permeabil-

Table 2. Pure gas permeability and selectivity for neat and mixed matrix membranes.

Membrane	Permeability (barrer)			Selectivity $\alpha(P_x/P_y)$	
	N_2	CH_4	CO_2	CO_2/N_2	CO_2/CH_4
PEEK-WC[65]	0.24	0.25	6.04	25.4	23.9
20% **C1**	0.10	0.20	4.10	42.1	20.8
20% **C2**	0.15	0.24	6.15	39.9	25.7
Matrimid®9725	0.31	0.35	10.8	35.5	31.1
20% **C1**	0.28	0.28	10.1	35.4	36.6
20% **C2**	0.51	0.40	16.7	32.7	41.7

Chemistry–A European Journal | Research Article
doi.org/10.1002/chem.202201631

Chemistry
Europe
European Chemical
Societies Publishing

Table 3. Diffusion coefficients and solubility for neat and mixed matrix membranes.

Membrane	Diffusivity [10^{-12} m^2 s^{-1}]			Solubility [cm$^3_{STP}$ cm^{-3} bar^{-1}]		
	N$_2$	CH$_4$	CO$_2$	N$_2$	CH$_4$	CO$_2$
PEEK-WC[65]	0.45	0.14	0.58	0.39	1.33	7.77
20% **C1**	0.68	0.15	0.59	0.11	0.95	5.19
20% **C2**	0.91	0.14	0.74	0.13	1.24	6.22
Matrimid®9725	1.12	0.19	0.84	0.20	1.32	9.59
20% **C1**	0.69	0.14	0.64	0.31	1.50	11.8
20% **C2**	1.22	0.22	1.21	0.31	1.38	10.4
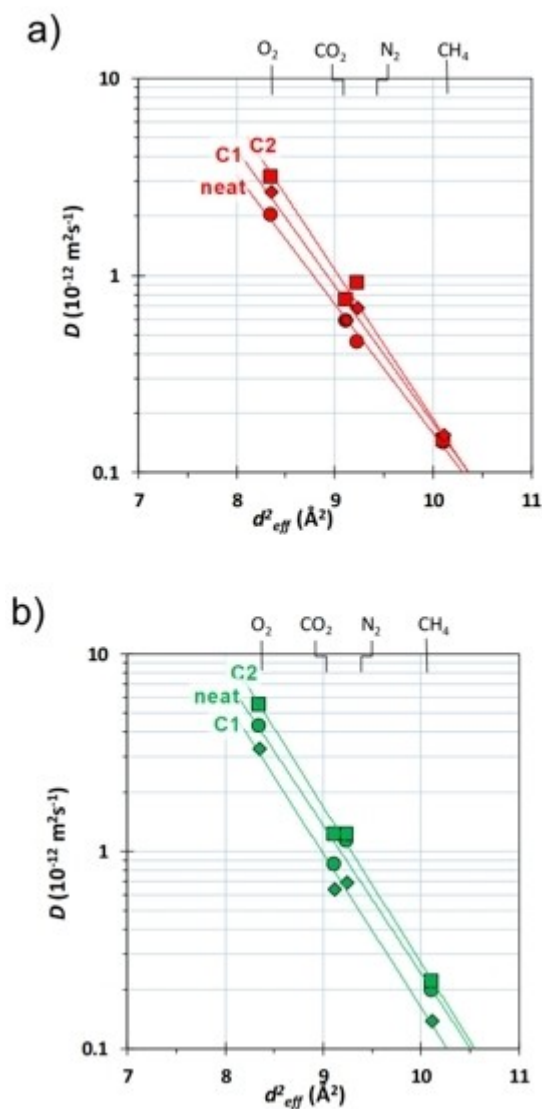
Figure 8. Correlation of the effective diffusion coefficient as a function of the molecular diameter[67] of four light gases in a) PEEK-WC and b) Matrimid® 9725. The various symbols are referred to: ●: Matrimid® 9725, ■: Matrimid® 9725/C2, ◆: Matrimid® 9725/C1, ●: PEEK-WC, ■: PEEK-WC/C2 and ◆: PEEK-WC/C1.

Adsorption studies with N$_2$ at 77 K suggest that the accessibility to pores is rather hindered in both **C1** and **C2**. This result is not surprising, considering the tight packing and the thick network of H-bonds revealed by crystal structures.

Gas-adsorption studies were also performed with CO$_2$, N$_2$ and CH$_4$ at 298 K. Notably, the BET surface areas calculated in these conditions from CO$_2$ resulted much higher than the values obtained with N$_2$ at 77 K. We could conclude that i) the **C1** and **C2** materials are more porous than expected from studies with N$_2$ at cryogenic temperature, ii) the cages framework is flexible enough to swell with increasing temperature.

C1 and **C2** were also successfully tested for potential CO$_2$/N$_2$ and CO$_2$/CH$_4$ separations in VSA processes. The good selectivity for CO$_2$ confirms that imide/imine groups strengthen the interaction with the quadrupolar CO$_2$ gas with respect to N$_2$ and CH$_4$ species.

C1 and **C2** also proved to be suitable as fillers for mixed-matrix membranes. Dense and robust MMMs were obtained from both cages with both PEEK-WC and Matrimid® 9725 polymers. Pure gas permeation tests with CO$_2$, N$_2$, and CH$_4$ gases showed an improvement in gas-transport properties compared to the pure polymer membranes. An increase in CO$_2$/CH$_4$ selectivity was found with **C1** and **C2** in Matrimid® 9725, whereas an increase in CO$_2$/N$_2$ selectivity was achieved with both cages in PEEK-WC.

Experimental Section

Deposition Numbers 2172063 (for **C1**-α), 2172064 (for **C2**-β), and 2172328 (for **C2**-d) contain the supplementary crystallographic data for this paper. These data are provided free of charge by the joint Cambridge Crystallographic Data Centre and Fachinformationszentrum Karlsruhe Access Structures service.

All the experimental details are reported in the Supporting Information.

Acknowledgements

showed that the **C1** material was mostly amorphous, whereas **C2** was obtained as a microcrystalline phase, although different from those crystallized from DMSO or MeCN, and characterized by SCXRD.

Chemistry–A European Journal

Research Article
doi.org/10.1002/chem.202201631

Chemistry Europe
European Chemical
Societies Publishing

Conflict of Interest

The authors declare no conflict of interest.

Data Availability Statement

The data that support the findings of this study are available from the corresponding author upon reasonable request.

Keywords: carbon capture · gas separation · mixed-matrix membranes · organic cages · porous materials

[1] T. Terlouw, K. Treyer, C. Bauer, M. Mazzotti, *Environ. Sci. Technol.* **2021**, *55*, 11397–11411.
[2] X. Wu, Y. Yu, Z. Qin, Z. Zhang, *Energy Prog.* **2014**, *63*, 1339–1346.
[3] M. Chawla, H. Saulat, M. Masood Khan, M. Mahmood Khan, S. Rafiq, L. Cheng, T. Iqbal, M. I. Rasheed, M. Z. Farooq, M. Saeed, et al., *Chem. Eng. Technol.* **2020**, *43*, 184–199.
[4] S. Kanehashi, C. A. Scholes, *Front. Chem.* **2020**, *14*, 460–469.
[5] J. Dechnik, J. Gascon, C. J. Doonan, C. Janiak, C. J. Sumby, *Angew. Chem. Int. Ed.* **2017**, *56*, 9292–9310; *Angew. Chem.* **2017**, *129*, 9420–9439.
[6] G. Zhang, B. Hua, A. Dey, M. Ghosh, B. A. Moosa, N. M. Khashab, *Acc. Chem. Res.* **2021**, *54*, 155–168.
[7] T. Tozawa, J. T. A. Jones, S. I. Swamy, S. Jiang, D. J. Adams, S. Shakespeare, R. Clowes, D. Bradshaw, T. Hasell, S. Y. Chong, et al., *Nat. Mater.* **2009**, *8*, 973–978.
[8] M. Mastalerz, *Acc. Chem. Res.* **2018**, *51*, 2411–2422.
[9] T. Kunde, T. Pausch, B. M. Schmidt, *Eur. J. Org. Chem.* **2021**, *2021*, 5844–5856.
[10] F. Beuerle, B. Gole, *Angew. Chem. Int. Ed.* **2018**, *57*, 4850–4878; *Angew. Chem.* **2018**, *130*, 4942–4972.
[11] M. Fang, C. Montoro, M. Semsarilar, *Membranes* **2020**, *10*, 107.
[12] A. J. Gosselin, C. A. Rowland, E. D. Bloch, *Chem. Rev.* **2020**, *120*, 8987–9014.
[13] J. D. Evans, D. M. Huang, M. R. Hill, C. J. Sumby, A. W. Thornton, C. J. Doonan, *J. Phys. Chem. C* **2014**, *118*, 1523–1529.
[14] A. F. Bushell, P. M. Budd, M. P. Attfield, J. T. a Jones, T. Hasell, A. I. Cooper, P. Bernardo, F. Bazzarelli, G. Clarizia, J. C. Jansen, *Angew. Chem. Int. Ed.* **2013**, *52*, 1253–1256; *Angew. Chem.* **2013**, *125*, 1291–1294.
[15] G. Zhu, F. Zhang, M. P. Rivera, X. Hu, G. Zhang, C. W. Jones, R. P. Lively, *Angew. Chem. Int. Ed.* **2019**, *58*, 2638–2643; *Angew. Chem.* **2019**, *131*, 2664–2669.
[16] A. Thevenet, A. Miljkovic, S. La Cognata, C. Marie, C. Tamain, N. Boubals, C. Mangano, V. Amendola, P. Guilbaud, *Dalton Trans.* **2021**, *50*, 1620–1630.
[17] S. La Cognata, R. Mobili, F. Merlo, A. Speltini, M. Boiocchi, T. Recca, L. J. Maher, V. Amendola, *ACS Omega* **2020**, 5, 26573–26582.
[18] R. Mobili, G. Preda, S. La Cognata, L. Toma, D. Pasini, V. Amendola, *Chem. Commun.* **2022**, *58*, 3897–3900.
[19] A. He, Z. Jiang, Y. Wu, H. Hussain, J. Rawle, M. E. Briggs, M. A. Little, A. G. Livingston, A. I. Cooper, *Nat. Mater.* **2022**, *21*, 463—470 .
[20] J. M. Lucero, M. A. Carreon, *ACS Appl. Mater. Interfaces* **2020**, *12*, 32182–32188.
[21] Z. M. Wang, Y. Y. Cui, C. X. Yang, X. P. Yan, *ACS Appl. Nano Mater.* **2020**, *3*, 479–485.
[22] M. Liu, L. Zhang, M. A. Little, V. Kapil, M. Ceriotti, S. Yang, L. Ding, D. L. Holden, R. Balderas-Xicohténcatl, D. He, et al., *Science* **2019**, *366*, 613–620.
[23] T. Hasell, A. I. Cooper, *Nat. Rev. Mater.* **2016**, *1*, 16053.
[24] M. C. Brand, F. Greenwell, R. Clowes, B. D. Egleston, A. Kai, A. I. Cooper, T. D. Bennett, R. L. Greenaway, *J. Mater. Chem. A* **2021**, *9*, 19807–19816.
[25] M. Mastalerz, *Chem. Eur. J.* **2012**, *18*, 10082–10091.
[26] A. Bavykina, A. Cadiau, J. Gascon, *Coord. Chem. Rev.* **2019**, *386*, 85–95.
[27] S. Ivanova, E. Köster, J. J. Holstein, N. Keller, G. H. Clever, T. Bein, F. Beuerle, *Angew. Chem. Int. Ed.* **2021**, *60*, 17455–17463.
[28] Y. Jin, B. A. Voss, R. D. Noble, W. Zhang, *Angew. Chem. Int. Ed.* **2010**, *49*, 6348–6351; *Angew. Chem.* **2010**, *122*, 6492–6495.
[29] J. C. Lauer, W. S. Zhang, F. Rominger, R. R. Schröder, M. Mastalerz, *Chem. Eur. J.* **2018**, *24*, 1816–1820.
[30] S. M. Elbert, N. I. Regenauer, D. Schindler, W. S. Zhang, F. Rominger, R. R. Schröder, M. Mastalerz, *Chem. Eur. J.* **2018**, *24*, 11438–11443.
[31] Y. Jin, C. Yu, R. J. Denman, W. Zhang, *Chem. Soc. Rev.* **2013**, *42*, 6634–6654.
[32] T. Kunde, E. Nieland, H. V. Schröder, C. A. Schalley, B. M. Schmidt, *Chem. Commun.* **2020**, *56*, 4761–4764.
[33] R. K. Gajula, R. Kishor, M. J. Prakash, *ChemistrySelect* **2019**, *4*, 12547–12555.
[34] F. Wang, E. Sikma, Z. Duan, T. Sarma, C. Lei, Z. Zhang, S. M. Humphrey, J. L. Sessler, *Chem. Commun.* **2019**, *55*, 6185–6188.
[35] M. Mastalerz, M. W. Schneider, I. M. Oppel, O. Presly, *Angew. Chem. Int. Ed.* **2011**, *50*, 1046–1051; *Angew. Chem.* **2011**, *123*, 1078–1083.
[36] W. Wang, K. Su, E. S. M. El-Sayed, M. Yang, D. Yuan, *ACS Appl. Mater. Interfaces* **2021**, *13*, 24042–24050.
[37] Q. Q. Wang, N. Luo, X. D. Wang, Y. F. Ao, Y. F. Chen, J. M. Liu, C. Y. Su, D. X. Wang, M. X. Wang, *J. Am. Chem. Soc.* **2017**, *139*, 635–638.
[38] H. Kim, Y. Kim, M. Yoon, S. Lim, S. M. Park, G. Seo, K. Kim, *J. Am. Chem. Soc.* **2010**, *132*, 12200–12202.
[39] Z. Wang, N. Sikdar, S. Q. Wang, X. Li, M. Yu, X. H. Bu, Z. Chang, X. Zou, Y. Chen, P. Cheng, et al., *J. Am. Chem. Soc.* **2019**, *141*, 9408–9414.
[40] H. H. Huang, K. S. Song, A. Prescimone, A. Aster, G. Cohen, R. Mannancherry, E. Vauthey, A. Coskun, T. Šolomek, *Chem. Sci.* **2021**, *12*, 5275–5285.
[41] A. L. Myers, J. M. Prausnitz, *AIChE J.* **1965**, *11*, 121–127.
[42] S. Jiang, J. Bacsa, X. Wu, J. T. A. Jones, R. Dawson, A. Trewin, D. J. Adams, A. I. Cooper, *Chem. Commun.* **2011**, *47*, 8919–8921.
[43] C. F. Macrae, I. J. Bruno, J. A. Chisholm, P. R. Edgington, P. McCabe, E. Pidcock, L. Rodriguez-Monge, R. Taylor, J. Van De Streek, P. A. Wood, *J. Appl. Crystallogr.* **2008**, *41*, 466–470.
[44] A. Lausi, M. Polentarutti, S. Onesti, J. R. Plaisier, E. Busetto, G. Bais, L. Barba, A. Cassetta, G. Campi, D. Lamba, et al., *Eur. Phys. J. Plus* **2015**, *130*, 43.
[45] J. Jeromenok, J. Weber, *Langmuir* **2013**, *29*, 12982–12989.
[46] M. Thommes, K. Kaneko, A. V. Neimark, J. P. Olivier, F. Rodriguez-Reinoso, J. Rouquerol, K. S. W. Sing, *Pure Appl. Chem.* **2015**, *87*, 1051–1069.
[47] M. Thommes, K. A. Cychosz, *Adsorption* **2014**, *20*, 233–250.
[48] D. Lozano-Castelló, D. Cazorla-Amorós, A. Linares-Solano, *Carbon* **2004**, *42*, 1233–1242.
[49] K. A. Cychosz, M. Thommes, *Engineering* **2018**, *4*, 559–566.
[50] K. C. Kim, T. U. Yoon, Y. S. Bae, *Microporous Mesoporous Mater.* **2016**, *224*, 294–301.
[51] M. Chen, B. Coasne, R. Guyer, D. Derome, J. Carmeliet, *Nat. Commun.* **2018**, *9*,3507.
[52] K. Wang, S. Qiao, X. Hu, *Sep. Purif. Technol.* **2004**, *34*, 165–176.
[53] H. Zhou, C. Rayer, A. R. Antonangelo, N. Hawkins, M. Carta, *ACS Appl. Mater. Interfaces* **2022**, *14*, 20997–21006.
[54] S. Lee, J. H. Lee, J. Kim, *Korean J. Chem. Eng.* **2018**, *35*, 214–221.

Chemistry–A European Journal

Research Article
doi.org/10.1002/chem.202201631

Chemistry Europe
European Chemical
Societies Publishing

[55] K. T. Leperi, R. Q. Snurr, F. You, *Ind. Eng. Chem. Res.* **2016**, *55*, 3338–3350.

[56] D. Lv, R. Shi, Y. Chen, Y. Chen, H. Wu, X. Zhou, H. Xi, Z. Li, Q. Xia, *Ind. Eng. Chem. Res.* **2018**, *57*, 12215–12224.

[57] B. Aghel, S. Behaein, S. Wongwises, M. S. Shadloo, *Biomass Bioenergy* **2022**, *160*, 106422.

[58] D. Lv, J. Y. Chen, K. Yang, H. Wu, Y. Chen, C. Duan, Y. Wu, J. Xiao, H. Xi, Z. Li, et al., *Chem. Eng. J.* **2019**, *375*, 122074.

[59] M. J. C. Ordoñez, K. J. Balkus, J. P. Ferraris, I. H. Musselman, *J. Membr. Sci.* **2010**, *361*, 28–37.

[60] J. C. Jansen, E. Drioli, *Polym. Sci. Ser. A* **2009**, *51*, 1355–1366.

[61] M. Monteleone, R. Mobili, C. Milanese, E. Esposito, A. Fuoco, S. La Cognata, V. Amendola, J. C. Jansen, *Molecules* **2021**, *26*, 5557.

[62] S. C. Fraga, M. Monteleone, M. Lanč, E. Esposito, A. Fuoco, L. Giorno, K. Pilnáček, K. Friess, M. Carta, N. B. McKeown, et al., *J. Membr. Sci.* **2018**, *561*, 39–58.

[63] L. M. Robeson, *J. Membr. Sci.* **1991**, *62*, 165–185.

[64] L. M. Robeson, *J. Membr. Sci.* **2008**, *320*, 390–400.

[65] E. Esposito, R. Bruno, M. Monteleone, A. Fuoco, J. Ferrando Soria, E. Pardo, D. Armentano, J. C. Jansen, *Appl. Sci.* **2020**, *10*, 1310.

[66] B. Comesaña-Gándara, J. Chen, C. G. Bezzu, M. Carta, I. Rose, M. C. Ferrari, E. Esposito, A. Fuoco, J. C. Jansen, N. B. McKeown, *Energy Environ. Sci.* **2019**, *12*, 2733–2740.

[67] V. Teplyakov, P. Meares, *Gas Sep. Purif.* **1990**, *4*, 66–74.